◆ Human Brain Mapping 35:1681–1690 (2014) ◆

Comprehensive Morphometry of Subcortical Grey Matter Structures in Early-Stage Parkinson's Disease

Ricarda A.L. Menke,[1,2,3]* Konrad Szewczyk-Krolikowski,[3,4] Saad Jbabdi,[1,4] Mark Jenkinson,[1,4] Kevin Talbot,[3,4] Clare E. Mackay,[1,2,3] and Michele Hu[3,4]

[1]*FMRIB Centre, Nuffield Department of Clinical Neurosciences, John Radcliffe Hospital, University of Oxford, Oxford, United Kingdom*
[2]*Department of Psychiatry, Warneford Hospital, University of Oxford, Oxford, United Kingdom*
[3]*Oxford Parkinson's Disease Centre (OPDC), University of Oxford, Oxford, United Kingdom*
[4]*Nuffield Department of Clinical Neurosciences, University of Oxford, Oxford, United Kingdom*

Abstract: Previous imaging studies that investigated morphometric group differences of subcortical regions outside the substantia nigra between non-demented Parkinson's patients and controls either did not find any significant differences, or reported contradictory results. Here, we performed a comprehensive morphometric analysis of 20 cognitively normal, early-stage PD patients and 19 matched control subjects. In addition to relatively standard analyses of whole-brain grey matter volume and overall regional volumes, we examined subtle localized surface shape differences in striatal and limbic grey matter structures and tested their utility as a diagnostic marker. Voxel-based morphometry and volumetric comparisons did not reveal significant group differences. Shape analysis, on the other hand, demonstrated significant between-group shape differences for the right pallidum. Careful diffusion tractography analysis showed that the affected parts of the pallidum are connected subcortically with the subthalamic nucleus, the pedunculopontine nucleus, and the thalamus and cortically with the frontal lobe. Additionally, microstructural measurements along these pathways, but not along other pallidal connections, were significantly different between the two groups. Vertex-wise linear discriminant analysis, however, revealed limited accuracy of pallidal shape for the discrimination between patients and controls. We conclude that localized disease-related changes in the right pallidum in early Parkinson's disease, undetectable using standard voxel-based morphometry or volumetry, are evident using sensitive shape analysis. However, the subtle nature of these changes makes it unlikely that shape analysis alone will be useful for early diagnosis. *Hum Brain Mapp 35:1681–1690, 2014.*

Key words: Parkinson's disease; MRI; segmentation; VBM; shape analysis; volumetry

Clare E. Mackay and Michele Hu contributed equally to this work.

Contract grant sponsors: Monument Discovery award from Parkinson's UK (the Parkinson's Disease Society of the United Kingdom); National Institute for Health Research (NIHR); NIHR Oxford Biomedical Research Centre; Thames Valley DeNDRoN (Dementias and Neurodegenerative Diseases Research Network).

*Correspondence to: Ricarda A.L. Menke, Centre for Functional MRI of the Brain (FMRIB), University of Oxford, Headley Way, Oxford OX3 9DU, United Kingdom. E-mail: ricarda@fmrib.ox.ac.uk

Received for publication 24 August 2012; Revised 1 January 2013; Accepted 13 February 2013

DOI: 10.1002/hbm.22282

Published online 16 July 2013 in Wiley Online Library (wileyonlinelibrary.com).

INTRODUCTION

Progressive degeneration of dopaminergic neurons in the substantia nigra (SN) pars compacta is one of the earliest pathological hallmarks of idiopathic Parkinson's disease (PD), thought to begin years before motor symptoms occur [Savica et al., 2010]. Additionally, neuroanatomical studies have revealed extensive extranigral neuropathological changes in sporadic PD, involving regions in the lower brain stem (such as the dorsal motor nucleus of the vagal nerves, raphe nuclei, locus coeruleus) as well as olfactory areas in the earliest (pre-motor) stages of the disease. Later, the disease process affects subnuclei of the amygdala and the thalamus, and eventually reaches the neocortex in the most advanced cases [Del Tredici et al., 2002]. Neuropathological changes in the SN are also likely to affect its dopaminergic projection sites such as the posterior putamen and caudate nucleus. The in vivo detection of early regional changes that accompany the PD disease process could assist early diagnosis of PD, and would therefore be a valuable tool in the clinical setting as well as the research context (i.e., for the development of neuroprotective therapies).

In the past, numerous magnetic resonance imaging (MRI) studies set out to find imaging correlates of volumetric changes in the SN or extra-nigral subcortical grey matter structures in non-demented idiopathic PD that might assist early diagnosis of the disease. Several studies measured the area of the SN in axial planes and reported significantly reduced SN width in PD [Minati et al., 2007; Pujol et al., 1992; Stern et al., 1989]. Significantly reduced volumes of the whole SN in PD have also been reported at 3T [Menke et al., 2009], but with limited specificity for diagnostic potential. Recently, two promising studies carried out at 7T field strength detected nigral boundary and volumetric differences in small samples of PD patients and controls [Cho et al., 2011; Kwon et al., 2012], suggesting that to date clinically elusive ultra-high field structural MRI that enables excellent visualization of the SN may be able to provide a diagnostic marker for PD in the future.

The few studies that have investigated extra-nigral PD-related grey matter changes in non-demented PD patients based on standard T1-weighted scans using either region of interest (usually basal ganglia or limbic structures) or voxel-based morphometry (VBM) approaches have produced inconclusive results. In particular, several VBM studies found no significant subcortical grey matter density differences [Burton et al., 2004; Focke et al., 2011; Jubault et al., 2009; Price et al., 2004], while others reported disease-related atrophy in the head of the left caudate nucleus [Brenneis et al., 2003] or in the right hippocampus [Summerfield et al., 2005]. The analysis of regional volumes, on the other hand, appears to be a more sensitive tool for the detection of PD-related subcortical grey matter changes than VBM analyses, but has also yielded inconsistent results. Some authors report volumetric differences for the caudate and the thalamus [Lee et al., 2011], or for the area of the caudate nucleus and the putamen [Kosta et al., 2006] after manual delineation, whereas others that utilized automated segmentation report no significant volume differences for putamen, caudate, pallidum, thalamus [Messina et al., 2011; Peran et al., 2010], hippocampus, or amygdala [Messina et al., 2011]. Despite the seemingly higher sensitivity for the identification of between group volume differences, manual segmentation suffers from inter-rater variability and is very labour intensive. Thus, in the context of imaging markers, a sensitive automated approach would be favourable.

Conceptually, the identification of localized areas of atrophy is likely to be more sensitive to subtle changes that might occur already in the early disease stages than assessing volumes of an entire brain structure. For example, Apostolova et al. used an automated machine-learning algorithm to segment the caudate and reported a trend towards reduced thickness for the right lateral caudate between cognitively normal PD patients and control subjects [Apostolova et al., 2010]. In the present study we aimed to conduct a comprehensive morphometric analysis of both cortical and deep grey matter structures in a group of early-stage cognitively healthy PD patients. In addition to comparing whole-brain grey matter morphometry and overall regional volumes between groups, we investigated, for the first time, surface shape differences in a variety of striatal and limbic grey matter structures between patients and a group of healthy, age and gender matched control subjects. Furthermore, for any structure that showed significant shape differences we conducted probabilistic tractography from the significant region to illustrate its connectivity and examine micro-structural differences within the respective pathways between the two groups. Lastly, we performed vertex-wise linear discriminant analysis with leave-one-out cross-validation to investigate the usefulness of vertex location as an early diagnostic marker for PD.

MATERIALS AND METHODS

Subjects

Twenty PD patients (9 female, 11 male) and twenty age- and sex-matched healthy subjects (9 female, 11 male) were recruited from the newly established Oxford Parkinson's Disease Centre (OPDC) cohort. The OPDC recruits patients from the Thames Valley area with a diagnosis of clinically probable idiopathic PD within the last 3 years according to UK PD Society Brain Bank criteria [Hughes et al., 1992]. Participants undergo extensive assessment in specially designated research clinics covering: general medical interview, detailed characterization of the motor and non-motor features of PD and cognitive assessment. The healthy control group consists of subjects unrelated to the PD patients recruited from spouses or friends of the PD participants. The experiments were undertaken with the understanding and written consent of each subject, with the approval from the local ethics committee, and in

TABLE I. Clinical information for the PD patient group

Score	Mean ± SD	Minimum	Maximum
Motor total	24.9 ± 10.0	8	42
UPDRS overall right	9.7 ± 5.8	1	18
UPDRS overall left	10.3 ± 6.2	0	21
Rigidity right	2.5 ± 1.1	1	4
Rigidity left	2.1 ± 1.6	0	5
Bradykinesia right	5.3 ± 3.8	0	12
Bradykinesia left	6.8 ± 4.3	0	13
Tremor right	1.8 ± 1.7	0	6
Tremor left	1.4 ± 1.2	0	4
Hoehn-Yahr	1.8 ± 0.4	1	2

Displayed are UPDRS scores ON medication. SD, standard deviation.

compliance with national legislation and the Declaration of Helsinki. Patients were scanned while taking their medication as usual, and motor function was assessed with the Unified Parkinson's Disease Rating Scale (UPDRS, Part III) and Hoehn and Yahr scales ON medication. To select a clinically homogenous patient group and minimize the risk of movement artefacts, we scanned only patients with predominantly akinetic-rigid Parkinsonism and minimal tremor, as can be seen from Table I. Cognition was assessed with the Mini-Mental State Examination (MMSE) [Folstein et al., 1975] and the Montreal Cognitive Assessment (MoCA) [Nasreddine et al., 2005].

Only subjects classified as cognitively healthy were included in the study. The respective inclusion criteria were MMSE>26 (which corresponds to no cognitive impairment in general population reference ranges [Crum et al., 1993; Tombaugh et al., 1992]), no subjective complaint of memory problems, and MoCA > 20.

Each subject's anatomical scan was checked for PD-unrelated gross structural abnormalities. One female healthy control subject presented with enlarged ventricles and had to be excluded from automated image analysis.

Data Acquisition

All MRI data were acquired on a 3T Siemens (Erlangen, Germany) Trio MR scanner with a 12-channel head coil.

For each subject T1-weighted images were obtained using a 3D Magnetization Prepared-Rapid Acquisition Gradient Echo (MP-RAGE) sequence (192 axial slices, flip angle: 8°, $1\times 1\times 1$ mm^3 voxel size, TE/TR/TI = 4.7 ms/2040 ms/900 ms). Acquisition time for the MP-RAGE image was 6 min.

In addition, whole-brain Fast Gray Matter Acquisition T1 Inversion Recovery (FGATIR, a contrast designed for the identification of subcortical structures for pre-surgical planning that enables clear visualization of the SN as a region of high signal intensity between the cerebral peduncles and the red nucleus) images [Sudhyadhom et al., 2009] (modified from the standard MP-RAGE sequence) were acquired (160 axial slices, flip angle: 8°, $0.9\times 0.9\times 1$ mm^3 voxel size, TE/TR/TI = 3.4 ms/3000 ms/409 ms). Acquisition time for the FGATIR data was 9 min.

Diffusion data were obtained using an echo planar imaging sequence (60 directions, b-value = 1,000 s/mm^2, TE/TR = 94 ms/9,300 ms, $2\times 2\times 2$ mm^3 voxel size, 65 slices). In addition, we acquired four images without diffusion weighting. A field map was acquired using a gradient echo imaging sequence ($2\times 2\times 2$ mm^3 voxel size, 65 slices, TE1/TE2/TR = 5.19 ms/7.65 ms/655 ms). Total acquisition time for the complete DTI data set was < 13 min.

Image Analysis

Analyses were performed using tools from the FMRIB Software Library (FSL) [Smith et al., 2004] (version 4.1).

Voxel-Based Morphometry

T1-weighted MP-RAGE data was analysed with FSL-VBM (part of FSL), a voxel-based morphometry style analysis [Ashburner and Friston, 2000; Good et al., 2001]. First, structural images were brain-extracted [Smith, 2002]. Next, tissue-type segmentation was carried out using FAST4 [Zhang et al., 2001]. The resulting grey matter partial volume images were then aligned to MNI152 standard space using the affine registration tool FLIRT [Jenkinson et al., 2002; Jenkinson and Smith, 2001], followed by nonlinear registration using FNIRT [Anderson et al., 2007]. The resulting images were averaged to create a study-specific template, to which the native grey matter images were then non-linearly re-registered. Since we had to discard one of the healthy control data sets due to enlarged ventricles, we randomly excluded one PD patient for the construction of the study-specific template to avoid any bias during the registration step caused by unequal sample sizes that could have favoured one of the groups. We then multiplied the registered partial volume images of all subjects by the Jacobian of the warp field ('modulation') to correct for local expansion or contraction. The modulated segmented images were then smoothed with an isotropic Gaussian kernel with a sigma of 3 mm. Voxel-wise GLM was applied using permutation-based non-parametric testing. Results were considered significant for $P < 0.05$, after correction for multiple comparisons (family wise error, FWE) using the TFCE approach [Smith and Nichols, 2009].

Assessment of Volume and Shape Differences of Subcortical Grey Matter Structures

Each subject's FGATIR image was skull-stripped [Smith, 2002] and aligned to the T1-weighted MP-RAGE image using affine registration. The left and right SN were manually segmented on the registered FGATIR images by one rater (RALM) who was blind to participant diagnosis and age at the time of the tracing. The SN was anatomically defined as an area of high signal between cerebral peduncles

and the red nucleus in the FGATIR images. Only parts of the SN that were visible on the same slices on which the red nucleus appeared were included. This approach has previously been shown to lead to good inter-rater reproducibility regarding the resulting volumes [Menke et al., 2009] and includes more than 80% of the dopaminergic neurons [Damier et al., 1999].

We segmented putamen, caudate, pallidum, thalamus, amygdala, and hippocampus from each subject's MP-RAGE image using FMRIB's Integrated Registration and Segmentation Tool (FIRST) [Patenaude et al., 2011].

For each subject brain tissue volume, normalized for subject head size, was estimated with SIENAX [Smith et al., 2002], part of FSL. SIENAX starts by extracting brain and skull images from the single whole-head input data. The brain image is then affine-registered to MNI152 space (using the skull image to determine the registration scaling); this is primarily in order to obtain the volumetric scaling factor, to be used for normalization for head size. Tissue-type segmentation with partial volume estimation is carried out in order to calculate total volume of brain tissue (including separate estimates of volumes of grey matter, white matter, peripheral grey matter and ventricular CSF).

The results of each step of the image processing, most importantly the subcortical segmentation, were carefully examined to ensure accuracy of the results.

Before conducting statistical analyses, the volumes of each subcortical region-of-interest were adjusted for inter-individual head size differences via multiplication by the volumetric scaling factor derived from SIENAX. All statistical analyses were carried out using IBM SPSS Statistics (Version 20) for Mac. Statistical comparisons between PD patients and healthy controls were carried out separately for the left and the right sides using nonparametric two independent samples t-tests. The significance level was set at < 0.05 (one-tailed).

Vertex analysis was performed using FIRST in a mode of operation that aims to assess group differences on a per-vertex basis by using a multi-variate General Linear Model. To normalize for inter-individual head size differences the meshes were reconstructed in MNI space. Following the per-vertex statistical analysis we performed False Discovery Rate (FDR) [Genovese et al., 2002] correction to address the issue of multiple comparisons in this vertex-wise analysis.

Post-Hoc Vertex-Wise Linear Discriminant Analysis for Vertices on the Surface of the Right Pallidum

To investigate the usefulness of individual vertex location as early diagnostic marker we performed vertex-wise linear discriminant analysis with leave-one-out cross-validation as implemented in FIRST for the structure that showed significant differences on the group level (FDR corrected).

Diffusion Tensor Imaging Data Preprocessing

Diffusion data were unwarped based on field map data with FUGUE, skull-stripped and then registered to a reference volume (the first acquired image without diffusion weighting) using affine registration [Jenkinson and Smith, 2001] to correct for eddy currents and head motion.

Fractional anisotropy (FA), mean diffusivity (MD), as well as axial (L1) and radial (L2/L3) diffusivity maps were generated using DTIFit within the FMRIB diffusion toolbox (part of FSL).

Voxel-wise estimates of fibre orientations and their uncertainty were calculated using FMRIB's Diffusion Toolbox (part of FSL), using a model that accounts for the possibility of crossing fibres within each voxel [Behrens et al., 2007]. We restricted the algorithm to estimating two fibre orientations at each voxel.

Post-Hoc Probabilistic Tractography From 'Significant' and 'Non-Significant' Vertices in the Right Pallidum

For each subject we extracted the coordinates for all vertices on the surface of the right pallidum that exceeded the FDR threshold ($P < 0.032$) in standard space (MNI 1mm). We then combined all these vertices into an image file using Matlab, which served as a seed mask for probabilistic tractography. The same procedure was used to seed masks from the non-significant vertices ($P > 0.050$).

Before running tractography, we registered each individual's FA map to the individual T1-weighted structural image using affine registration (FLIRT). In a second step, we transformed each subject's T1-weighted structural image to MNI 1mm space using non-linear registration (FNIRT). Finally, for each subject we combined the transformation matrix resulting from the affine registration and the warp field from the non-linear registration into a single warp field that contained the transformation from diffusion space to MNI 1mm space. This resulting warp field was then inverted, which enabled us to perform probabilistic tractography in standard space by feeding both warp fields into the tractography algorithm.

For each subject, tractography was run separately for two different seed masks: the mask of significant vertices and the mask of not-significant vertices In both cases, tractography was performed from every voxel in the respective seed mask generating 5,000 samples from each seed voxel to build up a connectivity distribution. For the tractography from the 'significant' voxels we discarded all pathways that entered any of the non-significant voxels (using the mask of the 'non-significant' voxels as an 'exclusion mask'), and vice versa. In both cases, to avoid bias caused by the close proximity of the putamen, we added the right putaminal surface as an exclusion mask.

Subsequently, for each individual subject (and both seed masks) the individual tractography maps were normalized by dividing the number of streamline samples present in

TABLE II. Normalized volumes of subcortical structures

Structure	PD patients	Control subjects
Right SN	499 ± 105	556 ± 144
Left SN	484 ± 112	533 ± 127
Right putamen	5,997 ± 782	5,817 ± 613
Left putamen	6,076 ± 879	5,966 ± 730
Right caudate	5,167 ± 611	5,145 ± 611
Left caudate	4,835 ± 560	4,925 ± 538
Right pallidum	1,952 ± 523	1,922 ± 448
Left pallidum	2,063 ± 539	1,955 ± 388
Right thalamus	8,003 ± 1039	8,014 ± 647
Left thalamus	8,000 ± 1028	8,076 ± 868
Right hippocampus	5,558 ± 703	5,568 ± 521
Left hippocampus	5,357 ± 851	5,340 ± 640
Right amygdala	1,479 ± 247	1,577 ± 424
Left amygdala	1,603 ± 260	1,548 ± 308

Volumes (mean ± standard deviation) are given in mm^3. PD, Parkinson's disease; SN, substantia nigra.

each voxel in the map by the 'waytotal', which corresponds to the total number of streamline samples that were not rejected due to the exclusion mask. The resulting maps were then thresholded to a value equal to 1% of the maximum voxel intensity value in the map and binarized.

Group-wise probabilistic maps were generated for both tracts (i.e., the tracts seeded from the 'significant' vertices and the tracts seeded from the 'non-significant' vertices) by averaging the respective binarized tract maps independently for the PD and the control group resulting in four different probabilistic tract maps. We then registered each subject's FA, MD, L1, L2, and L3 maps into standard space using the previously described transformations from diffusion space to MNI 1 mm space and thresholded all four probabilistic tracts maps at 60%. Finally, for the two different tracts (i.e., tracts seeded from the 'significant' vertices and tracts seeded from the 'not-significant' vertices) we extracted mean FA, MD, axial diffusivity (L1), and radial diffusivity (RD = (L2+L3)/2) values for each subject in a region-of-interest that contained only those voxels where the thresholded group maps for the PD group and the control group overlapped, and compared those values between the PD and the control group using nonparametric two independent samples *t*-tests. The significance level was set at < 0.05 (one-tailed and uncorrected).

RESULTS

Demographics and Clinical Information

Mean (± standard deviation, SD) age at the time of the MRI scan was 60 ± 11 years (range, 39–73) for the patient group and 60 ± 8 years (range, 41–75) for healthy control subjects. Mean MMSE was 28.9 ± 1.1 (range, 26–30) for the patient group and 29.5 ± 1.4 (range, 24–30) for healthy controls. The respective values for the MoCA score were 27.8 ± 1.8 (range, 23–30) for patients and 28.5 ± 1.3 (range, 26–30) for controls. There were no significant group differences in age, gender, MMSE, or MoCA. For the PD patient group, the mean disease duration between the time of (self-reported) disease onset and the time of MRI scan was 41.1 ± 18.9 months (range, 15.3–89.6). Mean disease duration since the time of clinical diagnosis was 1.8 ± 0.8 years (range, 0.4–3.0). All subjects were right-handed according to the Edinburgh Handedness Inventory [Oldfield, 1971]. 'ON' medication, motor symptom dominance was observed for the right side for 10 PD patients and for the left body half for nine patients. One patient's motor symptoms were symmetric. Additional detailed clinical information for the PD patients is presented in Table I.

Voxel-Based Morphometry

VBM of the grey matter did not yield any significant grey matter volume differences between the PD group and the control group.

Volumetry

There were no significant volumetric differences between PD patients and controls for any of the investigated structures. Mean volumes (± standard deviation) for all regions are displayed in Table II separately for the two different groups.

Shape Analysis of Subcortical Structures

Figure 1 illustrates the results of the vertex-wise shape comparisons between the PD and the control groups for those investigated subcortical structures that show significant group differences uncorrected for multiple comparisons ($P_{\text{uncorrected}} < 0.05$) across vertices for the right and the left hemisphere. For structures in the right hemisphere we observed between-group shape differences for the pallidum, putamen, hippocampus, and thalamus. For structures in the left hemisphere we observed shape differences only for the hippocampus and the thalamus. After correction for multiple comparisons, the only shape differences that remained significant were those for the right pallidum (FDR threshold was $P < 0.032$).

We did not observe any significant between-group shape differences for the caudate or the amygdala on either side.

Vertex-Wise Linear Discriminant Analysis for Right Pallidum Surface Voxels

The maximum discrimination accuracy was 71% for one vertex (74% sensitivity, 68% specificity), followed by 68% for two vertices (74% sensitivity, 63% specificity), and 66% for six vertices. The discrimination accuracies for the remaining vertices were 63% or below.

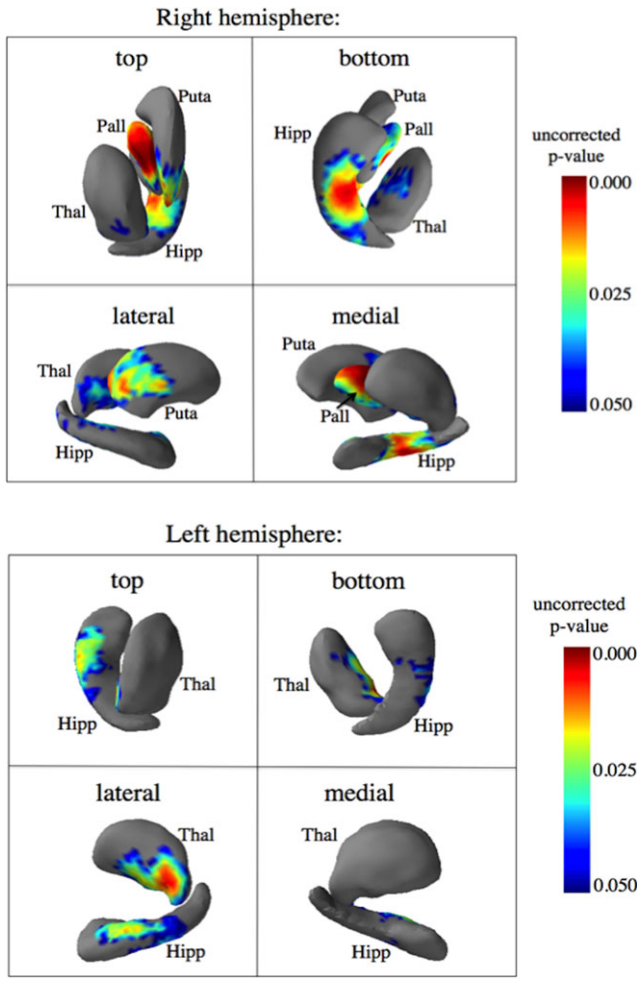

Figure 1.

Results of the vertex-wise shape comparisons between Parkinson's patients and controls for the right (top) and the left (bottom) hemisphere for those subcortical structures that show group differences ($P_{uncorrected} < 0.05$). Thal, thalamus; Pall, pallidum; Puta, putamen; Hipp, hippocampus. [Color figure can be viewed in the online issue, which is available at wileyonlinelibrary.com.]

Tractography From Right Pallidum Surface Voxels

Figure 2 shows the group maps that resulted from running tractography from 'significant' and 'non-significant' vertices on the surface of the right pallidum (thresholded to include at least 60% of the entire population for each map). Qualitatively, tracts seeded from the 'significant' vertices bypassed the subthalamic nucleus (STN) reaching down towards the location of the pedunculopontine nucleus (PPN; although note that this region could not be specifically identified on our MRI images), and were furthermore found to involve the fornix and parts of the anterior thalamic radiation, and to connect with the frontal lobe via the fronto-occipital fasciculus. Pathways seeded from the mask of 'non-significant' vertices were confined to the right cortico-spinal tract, covering widespread white matter regions spanning from the premotor cortex to the cerebral peduncles.

Statistical group comparisons of the mean values for the different DTI indices within the tract maps revealed significantly higher FA (controls: 0.382 ± 0.022, PD; 0.371 ± 0.027; $p = 0.027$) and significantly lower MD (controls: $8.42\times10^{-4} \pm 0.39\times10^{-4}$; PD: $8.67\times10^{-4} \pm 0.44\times10^{-4}$; $p = 0.033$) and radial diffusivity (controls: $6.69\times10^{-4} \pm 0.41\times10^{-4}$; PD: $6.97\times10^{-4} \pm 0.46\times10^{-4}$; $p = 0.028$) in the control group as compared with PD patients in the tracts seeded from the 'significant' vertices (Fig. 3). There were no significant group differences for any of the DTI measures within the tracts seeded from the 'non-significant' vertices.

DISCUSSION

This is the first study that compares surface shape differences in all disease-relevant striatal and limbic grey matter structures between early-stage PD patients and well-matched control subjects using a fully automated technique in addition to whole-brain grey matter density (VBM) and quantification of overall regional volumes.

As expected, vertex-wise analysis of shape differences following automated segmentation of subcortical grey matter structures proved to be more sensitive to subtle changes that occur in the early disease stages than VBM or volumetry, and demonstrated significant shape differences between PD patients and controls for the right pallidum. Post-hoc DTI tractography revealed that the respective significantly different vertices were mainly connected with the STN/SN and the PPN, as well as with the thalamus and the frontal lobe, pathways that are involved in PD in general, and in Parkinsonian akinesia in particular. In PD, the abnormal increase of activity of the STN caused by excessive inhibition of the lateral pallidum by the putamen in absence of dopamine is thought to cause the medial pallidum to inhibit the thalamus and thalamocortical pathway, resulting in reduced cortical activity that causes the typical motor disturbances [Albin et al., 1989; Wichmann and DeLong, 1996]. Furthermore, the descending basal ganglia projections to the pedunculopontine area in the upper brain stem seem to be particularly important in the genesis of akinesia. Clinical pallidotomy, for example, showed dramatic therapeutic effects on akinesia, that may be explained by interruption of amplified inhibitory output from the pallidum to brain stem regions such as the PPN [Iacono et al., 1995]. Furthermore, radiofrequency lesioning in the region of the PPN has been shown to cause akinesia in the normal monkey [Aziz et al., 1998; Munro-Davies et al., 1999], whereas injection of a GABA antagonist in the PPN significantly improved this symptom in MPTP-lesioned animals [Nandi et al., 2002]. Our patients had predominantly akinetic-rigid Parkinsonism with minimal tremor on motor testing, implicating

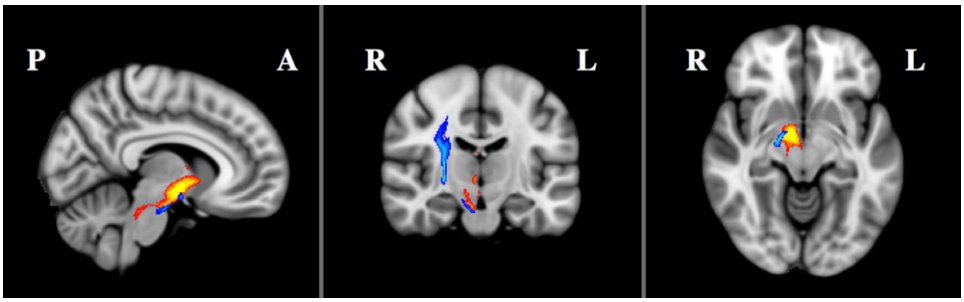

Figure 2.

Group maps (thresholded to include at least 60% of the entire ($n = 39$) population) that resulted from running tractography from vertices on the surface of the right pallidum in sagittal, coronal, and axial views. Red–yellow: Tractography from vertices that showed significant group differences after correction for multiple comparisons ($P < 0.032$). Blue–lightblue: Tractography from vertices that were not significantly different between groups ($P > 0.050$). P, posterior; A, anterior; R, right; L, left. [Color figure can be viewed in the online issue, which is available at wileyonlinelibrary.com.]

involvement of these akinesia-generating pathways. The fact that FA, MD, and the radial diffusivities L2 and L3 were found to be significantly different between the two groups only within the tracts seeded from the 'significant' vertices, but not in the pathways emerging from the 'non-significant' vertices, further corroborates the validity of the vertex analysis result.

The finding that only the right but not the left pallidum showed significant shape differences between PD patients and control subjects may reflect a trend towards significantly higher ipsilateral bradykinesia scores ($p_{\text{one-tailed}} = 0.055$; non-parametric independent samples t-test) for the nine patients with left-sided symptom dominance (mean bradykinesia score $\pm$ SD $= 9.8 \pm 3.0$) when compared with the 10 patients with right-sided symptom dominance (mean bradykinesia score 7.4 ± 3.6). Furthermore, all subjects included in our study were right-handed. Reports indicate that right-handedness might 'protect' left SN neurons [Cohen et al., 2003] and showing that dopamine levels are higher in the left than right striatum [Glick et al., 1982; van Dyck et al., 2002], potentially rendering the right hemisphere more susceptible to dopaminergic denervation [Haaxma et al., 2010] and its consequences. Therefore, in addition to the discussed asymmetry in motor features, handedness might have influenced the laterality of our result.

Also, the fact that we found more significant shape changes for the pallidum than for the putamen in our early-stage PD cohort may seem surprising. However, this seemingly counterintuitive result can be explained by looking at the shape analysis results more quantitatively (data not shown). While the mean differences between PD and control vertex locations are comparable for pallidum and putamen, the respective vertex-wise standard deviations are considerably higher for the putamen in the PD group than for the pallidum, leading to statistically stronger results for the latter structure.

Despite the significant differences on the group level, the results of the vertex-wise linear discriminant analysis for vertices on the surface of the right pallidum suggests that vertex location has limited potential as a diagnostic marker. Further work is required to investigate whether employing a higher resolution imaging protocol (possibly using higher magnetic field strength) might lead to

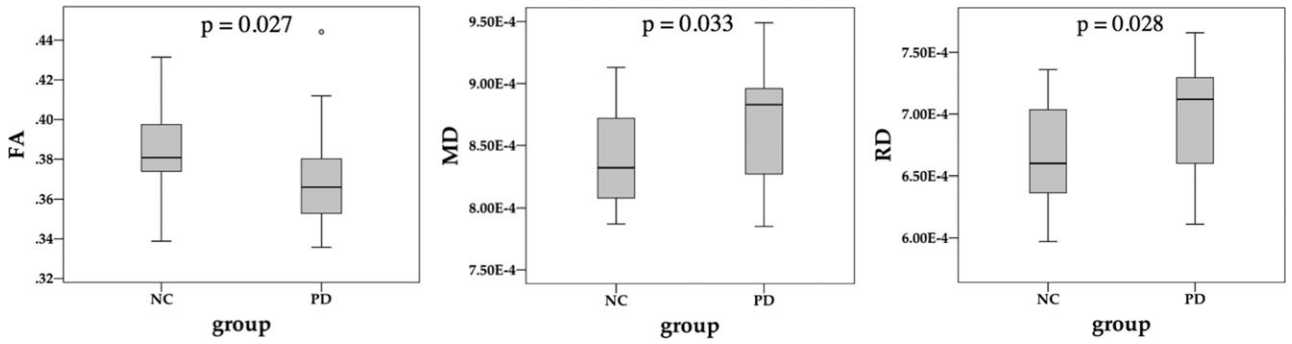

Figure 3.

DTI indices (averaged across the tracts seeded from the 'significant' vertices) that showed significant differences between Parkinson's patients (PD) and healthy control subjects (NC). FA, fractional anisotropy; MD, mean diffusivity; RD, radial diffusivity.

improved surface boundary identification and consequently improved classification accuracy. Neither VBM, nor subcortical region-of-interest volumetry showed significant grey matter differences between the two groups. The negative VBM result is in agreement with the majority of previously published studies that also reported no significant subcortical grey matter density differences between cognitively normal PD patients and healthy control subjects [Burton et al., 2004; Focke et al., 2011; Jubault et al., 2009; Price et al., 2004]. Similarly, the lack of significant volumetric group differences is in line with previous investigations of striatal and limbic volume differences following automated segmentation [Messina et al., 2011; Peran et al., 2010]. The use of manual segmentation has yielded more 'positive' results, such as reductions in caudate, thalamus and putamen volume in PD patients [Kosta et al., 2006; Lee et al., 2011]. Despite problems of subjectivity, this might be explained by generally higher segmentation accuracy for the manual approach as compared with automated segmentation.

In contrast to a previous study where we reported significantly smaller SN volumes in PD patients as compared to controls [Menke et al., 2009], the SN volume differences in the present study were more subtle and did not reach statistical significance. This is most likely due to the milder disease status and shorter disease duration of patients in the present study. Due to methodological limitations (lack of contrast on standard T1-weighted images), there is no model of the SN in FIRST [Patenaude et al., 2011], and thus it was not possible to investigate between group vertex-wise surface shape comparisons for the left and right SN. The pathological involvement of the SN is thought to precede the involvement of the other subcortical grey matter structures that were analysed using shape analysis in our study [Del Tredici et al., 2002], making this region one of the most promising candidates in search of an early diagnostic marker for PD. In contrast to the other subcortical grey matter regions that were investigated in this study, the SN was segmented manually. The transformation of an image file resulting from manual segmentation (SN masks) into a surface mesh representation that can be utilized for vertex analysis implemented in FIRST is currently under development, and might show strong localized nigral shape differences between early PD and controls which could have diagnostic potential.

In common with all similar studies, our investigation is limited by the lack of pathological confirmation of the disease status for our patient cohort, in particular because the selection of early-stage PD patients bears the risk of including patients with atypical Parkinsonism. However, all patients were diagnosed with clinically probable idiopathic PD according to UK PD Society Brain Bank criteria [Hughes et al., 1992], and undergo longitudinal clinical evaluation with reassessment of their diagnosis over time.

Furthermore, the investigation of patients in the earliest disease stages is a necessity in search of markers that might enable the identification of the preclinical phase, which is vital for the development and eventual application of neuroprotective treatments.

Other limitations include the relatively small sample size, which may have reduced the sensitivity to detect subtle morphometric differences on the group level, as well as the patient selection that might cause our results to be more relevant to the akinetic-rigid phenotype.

CONCLUSIONS

We conducted a comprehensive analysis of subcortical morphometry in early-stage PD and found subtle differences in pallidal shape that appear to project to known disease-related structures. As such, shape analysis may contribute to our understanding of the early mechanisms of Parkinson's disease. However, despite the use of sensitive, state-of-the-art MRI protocols and analysis tools the findings were subtle and did not produce reasonable accuracy scores for diagnosis on an individual level. Without a step-change in technology, techniques such as volumetry, voxel-based morphometry, and vertex-wise analysis of surface shape differences are unlikely to provide a useful marker for the early diagnosis of early PD.

ACKNOWLEDGMENTS

The authors are indebted to all patients and healthy control subjects who participated in our study.

REFERENCES

Albin RL, Young AB, Penney JB (1989): The functional anatomy of basal ganglia disorders. Trends Neurosci 12:366–375.

Anderson JLR, Andersson M, Jenkinson M, Smith S (2007): Non-linear registration, aka Spatial normalisation.

Apostolova LG, Beyer M, Green AE, Hwang KS, Morra JH, Chou YY, Avedissian C, Aarsland D, Janvin CC, Larsen JP, Cummings JL, Thompson PM (2010): Hippocampal, caudate, and ventricular changes in Parkinson's disease with and without dementia. Mov Disord 25:687–695.

Ashburner J, Friston KJ (2000): Voxel-based morphometry—The methods. Neuroimage 11:805–821.

Aziz TZ, Davies L, Stein J, France S (1998): The role of descending basal ganglia connections to the brain stem in parkinsonian akinesia. Br J Neurosurg 12:245–249.

Behrens TEJ, Berg HJ, Jbabdi S, Rushworth MFS, Woolrich MW (2007): Probabilistic diffusion tractography with multiple fibre orientations: What can we gain? Neuroimage 34:144–155.

Brenneis C, Seppi K, Schocke MF, Muller J, Luginger E, Bosch S, Loscher WN, Buchel C, Poewe W, Wenning GK (2003): Voxel-based morphometry detects cortical atrophy in the Parkinson variant of multiple system atrophy. Mov Disord 18:1132–1138.

Burton EJ, McKeith IG, Burn DJ, Williams ED, O'Brien JT (2004): Cerebral atrophy in Parkinson's disease with and

without dementia: A comparison with Alzheimer's disease, dementia with Lewy bodies and controls. Brain 127:791–800.

Cho ZH, Oh SH, Kim JM, Park SY, Kwon DH, Jeong HJ, Kim YB, Chi JG, Park CW, Huston J, III, Lee KH, Jeon BS (2011): Direct visualization of Parkinson's disease by in vivo human brain imaging using 7.0T magnetic resonance imaging. Mov Disord 26:713–718.

Cohen AD, Tillerson JL, Smith AD, Schallert T, Zigmond MJ (2003): Neuroprotective effects of prior limb use in 6-hydroxydopamine-treated rats: Possible role of GDNF. J Neurochem 85:299–305.

Damier P, Hirsch EC, Agid Y, Graybiel AM (1999): The substantia nigra of the human brain. II. Patterns of loss of dopamine-containing neurons in Parkinson's disease. Brain 122 (Part 8):1437–1448.

Del Tredici K, Rub U, De Vos RAI, Bohl JRE, Braak H (2002): Where does parkinson disease pathology begin in the brain? J Neuropathol Exp Neurol 61:413–426.

Focke NK, Helms G, Scheewe S, Pantel PM, Bachmann CG, Dechent P, Ebentheuer J, Mohr A, Paulus W, Trenkwalder C (2011): Individual voxel-based subtype prediction can differentiate progressive supranuclear palsy from idiopathic Parkinson syndrome and healthy controls. Hum Brain Mapp 32:1905–1915.

Folstein MF, Folstein SE, McHugh PR (1975): Mini-mental state. A practical method for grading the cognitive state of patients for the clinician. J Psychiatr Res, 12:189–198.

Genovese CR, Lazar NA, Nichols T (2002): Thresholding of statistical maps in functional neuroimaging using the false discovery rate. Neuroimage 15:870–878.

Glick SD, Ross DA, Hough LB (1982): Lateral asymmetry of neurotransmitters in human brain. Brain Res 234:53–63.

Good CD, Johnsrude IS, Ashburner J, Henson RN, Friston KJ, Frackowiak RS (2001): A voxel-based morphometric study of ageing in 465 normal adult human brains. Neuroimage 14:21–36.

Haaxma CA, Helmich RC, Borm GF, Kappelle AC, Horstink MW, Bloem BR (2010): Side of symptom onset affects motor dysfunction in Parkinson's disease. Neuroscience 170:1282–1285.

Hughes AJ, Daniel SE, Kilford L, Lees AJ (1992): Accuracy of clinical diagnosis of idiopathic Parkinson's disease: A clinico-pathological study of 100 cases. J Neurol Neurosurg Psychiatry 55:181–184.

Iacono RP, Lonser RR, Ulloth JE, Shima F (1995): Postero-ventral pallidotomy in Parkinson's disease. J Clin Neurosci 2:140–145.

Jenkinson M, Smith S (2001): A global optimisation method for robust affine registration of brain images. Med Image Anal 5:143–156.

Jenkinson M, Bannister P, Brady M, Smith S (2002): Improved optimization for the robust and accurate linear registration and motion correction of brain images. Neuroimage 17:825–841.

Jubault T, Brambati SM, Degroot C, Kullmann B, Strafella AP, Lafontaine A-L, Chouinard S, Monchi O (2009): Regional brain stem atrophy in idiopathic Parkinson's disease detected by anatomical MRI. PLoS One 4:e8247.

Kosta P, Argyropoulou MI, Markoula S, Konitsiotis S (2006): MRI evaluation of the basal ganglia size and iron content in patients with Parkinson's disease. J Neurol 253:26–32.

Kwon DH, Kim JM, Oh SH, Jeong HJ, Park SY, Oh ES, Chi JG, Kim YB, Jeon BS, Cho ZH (2012): Seven-Tesla magnetic resonance images of the substantia nigra in Parkinson disease. Ann Neurol 71:267–277.

Lee SH, Kim SS, Tae WS, Lee SY, Choi JW, Koh SB, Kwon DY (2011): Regional volume analysis of the Parkinson disease brain in early disease stage: Gray matter, white matter, striatum, and thalamus. AJNR Am J Neuroradiol 32:682–687.

Menke RA, Scholz J, Miller KL, Deoni S, Jbabdi S, Matthews PM, Zarei M (2009): MRI characteristics of the substantia nigra in Parkinson's disease: A combined quantitative T1 and DTI study. Neuroimage 47:435–441.

Messina D, Cerasa A, Condino F, Arabia G, Novellino F, Nicoletti G, Salsone M, Morelli M, Lanza PL, Quattrone A (2011): Patterns of brain atrophy in Parkinson's disease, progressive supranuclear palsy and multiple system atrophy. Parkinsonism Relat Disord 17:172–176.

Minati L, Grisoli M, Carella F, De Simone T, Bruzzone MG, Savoiardo M (2007): Imaging degeneration of the substantia nigra in Parkinson disease with inversion-recovery MR imaging. AJNR Am J Neuroradiol 28:309–313.

Munro-Davies LE, Winter J, Aziz TZ, Stein JF (1999): The role of the pedunculopontine region in basal-ganglia mechanisms of akinesia. Exp Brain Res 129:511–517.

Nandi D, Aziz TZ, Giladi N, Winter J, Stein JF (2002): Reversal of akinesia in experimental parkinsonism by GABA antagonist microinjections in the pedunculopontine nucleus. Brain 125:2418–2430.

Nasreddine ZS, Phillips NA, Bedirian V, Charbonneau S, Whitehead V, Collin I, Cummings JL, Chertkow H (2005): The Montreal Cognitive Assessment, MoCA: A brief screening tool for mild cognitive impairment. J Am Geriatr Soc 53:695–699.

Oldfield RC (1971): The assessment and analysis of handedness: The Edinburgh inventory. Neuropsychologia 9:97–113.

Patenaude B, Smith SM, Kennedy DN, Jenkinson M (2011): A Bayesian model of shape and appearance for subcortical brain segmentation. Neuroimage 56:907–922.

Peran P, Cherubini A, Assogna F, Piras F, Quattrocchi C, Peppe A, Celsis P, Rascol O, Demonet JF, Stefani A, Pierantozzi M, Pontieri FE, Caltagirone C, Spalletta G, Sabatini U (2010): Magnetic resonance imaging markers of Parkinson's disease nigrostriatal signature. Brain 133:3423–3433.

Price S, Paviour D, Scahill R, Stevens J, Rossor M, Lees A, Fox N (2004): Voxel-based morphometry detects patterns of atrophy that help differentiate progressive supranuclear palsy and Parkinson's disease. Neuroimage 23:663–669.

Pujol J, Junque C, Vendrell P, Grau JM, Capdevila A (1992): Reduction of the substantia nigra width and motor decline in aging and Parkinson's disease. Arch Neurol 49:1119–1122.

Savica R, Rocca WA, Ahlskog JE (2010): When does Parkinson disease start? Arch Neurol 67:798–801.

Smith S, Nichols T (2009): Threshold-free cluster enhancement: Addressing problems of smoothing, threshold dependence and localisation in cluster inference. Neuroimage 44:83–98.

Smith SM (2002): Fast robust automated brain extraction. Hum Brain Mapp 17:143–155.

Smith SM, Zhang Y, Jenkinson M, Chen J, Matthews PM, Federico A, De Stefano N (2002): Accurate, robust, and automated longitudinal and cross-sectional brain change analysis. Neuroimage 17:479–489.

Smith SM, Jenkinson M, Woolrich MW, Beckmann CF, Behrens TEJ, Johansen-Berg H, Bannister PR, De Luca M, Drobnjak I, Flitney DE, Niazy RK, Saunders J, Vickers J, Zhang Y, De Stefano N, Brady JM, Matthews PM (2004): Advances in functional and structural MR image analysis and implementation as FSL. Neuroimage 23 (Suppl 1):S208–S219.

Stern MB, Braffman BH, Skolnick BE, Hurtig HI, Grossman RI (1989): Magnetic resonance imaging in Parkinson's disease and parkinsonian syndromes. Neurology 39:1524–1526.

Sudhyadhom A, Haq IU, Foote KD, Okun MS, Bova FJ (2009): A high resolution and high contrast MRI for differentiation of subcortical structures for DBS targeting: the Fast Gray Matter Acquisition T1 Inversion Recovery (FGATIR). Neuroimage 47 (Suppl 2):T44–T52.

Summerfield C, Junque C, Tolosa E, Salgado-Pineda P, Gomez-Anson B, Marti MJ, Pastor P, Ramirez-Ruiz B, Mercader J (2005): Structural brain changes in Parkinson disease with dementia: A voxel-based morphometry study. Arch Neurol 62:281–285.

van Dyck CH, Seibyl JP, Malison RT, Laruelle M, Zoghbi SS, Baldwin RM, Innis RB (2002): Age-related decline in dopamine transporters: Analysis of striatal subregions, nonlinear effects, and hemispheric asymmetries. Am J Geriatr Psychiatry 10:36–43.

Wichmann T, DeLong MR (1996): Functional and pathophysiological models of the basal ganglia. Curr Opin Neurobiol 6:751–758.

Zhang Y, Brady M, Smith S (2001): Segmentation of brain MR images through a hidden Markov random field model and the expectation-maximization algorithm. IEEE Trans Med Imaging 20:45–57.